Nano Research
DOI 10.1007/s12274-014-0486-z
Research Article
ISSN 1998-0124
CN 11-5974/O4

High thermal conductivity of suspended few-layer hexagonal boron nitride sheets

Haiqing Zhou[1,3], Jixin Zhu[2,4], Zheng Liu[4], Zheng Yan[1], Xiujun Fan[1], Jian Lin[2,5], Gunuk Wang[1], Qingyu Yan[4] (✉), Ting Yu[3] (✉), Pulickel M. Ajayan[2,5](✉), and James M. Tour[1,2,5] (✉)

Nano Res., **Just Accepted Manuscript** • DOI: 10.1007/s12274-014-0486-z
http://www.thenanoresearch.com on April 25, 2014

Just Accepted

TABLEOF CONTENTS (TOC)

High thermal conductivity of suspended few-layer hexagonal boron nitride sheets

Haiqing Zhou[1,3], Jixin Zhu[2,4], Zheng Liu[4], Zheng Yan[1], Xiujun Fan[1], Jian Lin[2,5], Gunuk Wang[1], Qingyu Yan[4,*], Ting Yu[3,*], Pulickel M. Ajayan[2,5,*] and James M. Tour[1,2,5,*]

[1]Rice University, United States
[2]Rice University, United States
[3]Nanyang Technological University, Singapore
[4]Nanyang Technological University, Singapore
[5]Rice University, United States

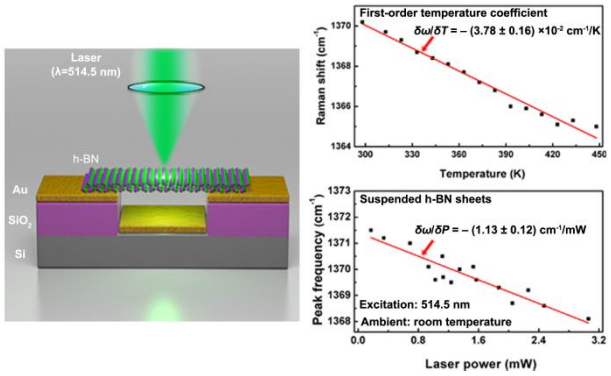

We report the experimental investigation of thermal conduction in suspended few-layer h-BN sheets using a noncontact micro-Raman spectroscopy method. The first-order temperature coefficients for 1L, 2L and 9L h-BN sheets were found to be $-(3.41 \pm 0.12) \times 10^{-2}$, $-(3.15 \pm 0.14) \times 10^{-2}$ and $-(3.78 \pm 0.16) \times 10^{-2}$ cm^{-1}/K, respectively. The room-temperature thermal conductivity of few-layer h-BN sheets was found to be around 243 $Wm^{-1}K^{-1}$, which was comparable to that of bulk h-BN, indicating their potential use as important components to solve heat dissipation problems in thermal management configurations.

Provide the authors' webside if possible.

Author 1, webside 1

Author 2, webside 2

Nano Res
DOI (automatically inserted by the publisher)
Research Article

High thermal conductivity of suspended few-layer hexagonal boron nitride sheets

Haiqing Zhou[1,3], Jixin Zhu[2,4], Zheng Liu[4], Zheng Yan[1], Xiujun Fan[1], Jian Lin[2,5], Gunuk Wang[1], Qingyu Yan[4] (✉), Ting Yu[3] (✉), Pulickel M. Ajayan[2,5](✉), and James M. Tour[1,2,5] (✉)

[1] Department of Chemistry, Rice University, 6100 Main Street, Houston, Texas 77005, United States
[2]Department of Materials Science and NanoEngineering, Rice University, 6100 Main Street, Houston, Texas 77005, United States
[3]Division of Physics and Applied Physics, School of Physical and Mathematical Sciences, Nanyang Technological University, 637371, Singapore
[4]School of Materials Science and Engineering, Nanyang Technological University, Nanyang Avenue, 639798,Singapore
[5]The Smalley Institute for Nanoscale Science and Technology, Rice University, 6100 Main Street, Houston, Texas 77005, United States

Received: day month year / Revised: day month year / Accepted: day month year (automatically inserted by the publisher)

ABSTRACT

The thermal conduction of suspended few-layer h-BN sheets was experimentally investigated using a noncontact micro-Raman spectroscopy method. The first-order temperature coefficients for 1L, 2L and 9L h-BN sheets were measured to be – (3.41 ± 0.12) × 10^{-2}, – (3.15 ± 0.14) × 10^{-2} and – (3.78 ± 0.16) × 10^{-2} cm^{-1}/K, respectively. The room-temperature thermal conductivity of few-layer h-BN sheets was found to be 243 + 37/- 16 $Wm^{-1}K^{-1}$, which was comparable to that of bulk h-BN, indicating their potential use as important components to solve heat dissipation problems in thermal management configurations.

KEYWORDS

Two-dimensional, hexagonal boron nitride (h-BN), thermal conductivity, Raman spectroscopy

1. Introduction

Hexagonal boron nitride (h-BN) is a common nontoxic material used for its low electrical conductivity, high thermal conductivity, and superior lubricant properties. Analogous to graphene, h-BN is a two-dimensional (2D) honeycomb-structured crystal, in which an equal number of alternating B and N atoms are covalently bonded with sp^2 hybridization and yet demonstrate remarkable ionic character[1-3]. Recently, h-BN has been found to be an important 2D crystal and dielectric gate substrate for graphene because the atomically smooth surface and strong bonding of h-BN significantly improves

Address correspondence to tour@rice.edu; ajayan@rice.edu; yuting@ntu.edu.sg; alexyan@ntu.edu.sg

carrier mobilities in graphene by a factor of 10 when compared to those of graphene on SiO_2[3-5]. Furthermore, compared to SiO_2, h-BN is an appealing dielectric substrate for graphene devices because its atomically smooth surface is relatively free of dangling bonds and charge traps, which leads to weak electronic interlayer coupling between graphene and h-BN sheets, and thus preserves the electronic and optical properties intrinsic to graphene[3-6]. Due to its geometric similarity, h-BN possesses some physical properties similar to graphene, such as strong mechanical properties[7,8] and high chemical and thermal stability[7,9-11]. Given that the strong bonding of atoms such as C-C and B-N results in a large phonon contribution, as exemplified in BN, carbon nanotubes and graphene, it is expected that the h-BN crystal could have a high thermal conductivity[12-15]. However, recent research on h-BN mainly focuses on its large-scale synthesis[16-20] and optical and electronic properties[1-3,5,21,22] rather than the thermal properties[23]. Therefore, motivated by the superior thermal conductivity of graphene, it is imperative to determine whether h-BN sheets also possess high thermal conductivity, thus better understanding its properties as a component in electrical and thermal management devices.

With the decrease in feature sizes of microelectronic devices and circuits, the dissipation power density significantly increases. Consequently, efficient heat removal or conduction becomes a crucial design characteristic for next-generation integrated circuits, electronic and optoelectronic devices, in which thermal conduction is a key limiting factor to further device miniaturization. It is known that traditional Si-based semiconductors show a dramatic suppression of thermal conductivity at the nanometer scale, while insulators such as Si_3N_4, SiO_2, and Al_2O_3 used in microelectronic devices are all poor thermal conductors in their usual forms. But for bulk h-BN, it is interesting to note that its thermal conductivity is ~ 390 $Wm^{-1}K^{-1}$, which is 280 times larger than that of SiO_2. For thin h-BN sheets, the thermal conductivity value could exceed or be comparable to that of its bulk crystalline form[14,15]. In addition, because layered h-BN is an electrical insulator with a wide band-gap (5.5 ~ 6.0 eV), chemical inertness and possibly good thermal conductivity, integrating h-BN with graphene has become a common approach to experimental device fabrication. Hence it is desirable to find a suitable, simple method to evaluate the thermal conductivity of thin h-BN sheets. The synthesis of large-scale and highly crystalline h-BN sheets with controlled layers via low pressure chemical vapor deposition (LPCVD) has been demonstrated[8,24-26], thereby providing an opportunity to explore the thermal conductivity of h-BN sheets.

In the present work, using confocal micro-Raman spectroscopy, a nondestructive and unconventional approach for the noncontact measurement of the thermal conductivity of suspended h-BN sheets synthesized by a LPCVD method was demonstrated. The Raman spectra of monolayer (1L), bilayer (2L) and 9-layer (9L) h-BN sheets were found to be dependent on the surrounding temperature, and the peak frequencies of the Raman E_{2g} mode vary linearly with temperature. The first-order temperature coefficients of the Raman E_{2g} mode for these samples were: $(3.41 \pm 0.12) \times 10^{-2}$; $(3.15 \pm 0.14) \times 10^{-2}$ and $(3.78 \pm 0.16) \times 10^{-2}$ cm^{-1}/K, respectively. The thermal conductivity of suspended 9L h-BN sheets at room temperature was around 243 $Wm^{-1}K^{-1}$, which was comparable to that of bulk h-BN, indicating its potential use in components for heat dissipation in thermal management, especially when the 9L h-BN serves as a dielectric gate substrate for graphene/h-BN integrated nanodevices.

2. Experimental

For the growth of h-BN [26], 12.5 μm thick Ni foils (Goodfellow, Inc. Purity: 99.9%) were placed in the centre of a tube furnace and gradually heated to 950 °C over 40 min and was then annealed at 950 °C for 10 min in 500 sccm Ar/H_2 gas flow (15 vol% H_2 balanced by 85 vol%Ar) with a chamber pressure ~ 800 mTorr. Subsequently, the furnace was gradually heated to 1000 °C in 10 min. Ammonia borane (NH_3-BH_3) was sublimed at 130 °C using a heating element and the gas was carried into the reaction zone by the Ar/H_2 carrier gas. During the growth process, the total flow of mixed Ar/H_2 gas (15 vol% H_2 balanced by 85 vol% argon) was kept at 300 sccm

with a pressure ~ 400 mTorr and the thickness of h-BN was controlled by changing the growth time (7 min for 1L, 10 min for 2L and 20 min for 9L). After the growth, the furnace was quickly cooled to room temperature. As reported in our previous work[8,24-26], the as-grown h-BN films on Ni foils were removed from the furnace, and spin-coated with a thin film of poly(methyl methacrylate) (PMMA, MicroChem Corp. 950 PMMA A4, 4% in anisole) atop. The underlying Ni substrate was dissolved in a dilute nitric acid solution. Then the films were transferred to other substrates for further characterizations after the removal of the thin PMMA film by soaking in acetone for 30 min.

The micro-Raman spectroscopy (Renishaw inVia Raman Spectroscope) experiments were carried out under ambient conditions using 514.5 nm laser excitation with a laser spot size ~ 1μm. During the measurements of temperature-dependent Raman spectra, the laser power was set below 0.5 mW so as to avoid local laser heating on samples. Many Raman spectra (~ 10) of h-BN sheets were collected to ensure the credibility and repeatability of the results.

3. Results and discussion

The h-BN sheets used here were grown on 12.5 μm thick nickel foils using a LPCVD method that was previously reported[8,24-26]. We transferred the as-grown samples onto the 150 nm Au film-coated silicon substrate with many pre-patterned trenches for measuring thermal conductivity. The details are shown in the Supporting Information. Some of the h-BN films were transferred onto silicon substrates for further characterization. Before thermal transport measurements, the uniformity and quality of the h-BN samples were examined by optical microscopy (OM), Raman spectroscopy, scanning electron microscopy (SEM), atomic force microscopy (AFM) and X-ray photoelectron spectroscopy (XPS) as shown in Figure 1 and Figures S1 and S2. In order to differentiate the transferred h-BN film from the silicon substrate, a trench was scratched using a tweezer, marked by a white arrow in Figure 1a. As is indicated in the optical image (Figure 1a), the h-BN film is mainly 2L, as confirmed by the AFM (Figure S1) and following TEM characterizations. The typical height of the h-BN film was ~ 1 nm as indicated in the Figure S1 inset. There are some areas that are marked by blue arrows, which appear to be 1L h-BN sheet (Figure 1a). The color contrast between these thin regions and the silicon substrate is nearly undetectable[19]. However, an obvious Raman signal with a Raman peak located at 1370 cm^{-1} (corresponding to the vibration E_{2g} mode of h-BN) can be identified in the regions marked by blue arrows, indicating it is from 1L h-BN. The Raman spectra of layered materials are sensitive to their quality and film thickness. In order to correlate the Raman signal to the thickness of the h-BN, we have recorded the Raman spectra from different thicknesses of the CVD-grown h-BN sheets that have been placed on silicon substrates with a 285-nm-thick SiO_2 layer (Figure 1b). It is found that the peak intensities of the Raman E_{2g} mode ~ 1370 cm^{-1} are strongly related to the h-BN thickness and increase with an increase inlayer number. In addition, the peak position of bulk h-BN shifts toward lower frequency compared to 1L, 2L and thin h-BN sheets (~ 9 layers as determined by TEM characterization, vide infra). These Raman signatures are consistent with those reported for mechanically exfoliated h-BN sheets[27], indicating the high quality and crystallinity of the samples.

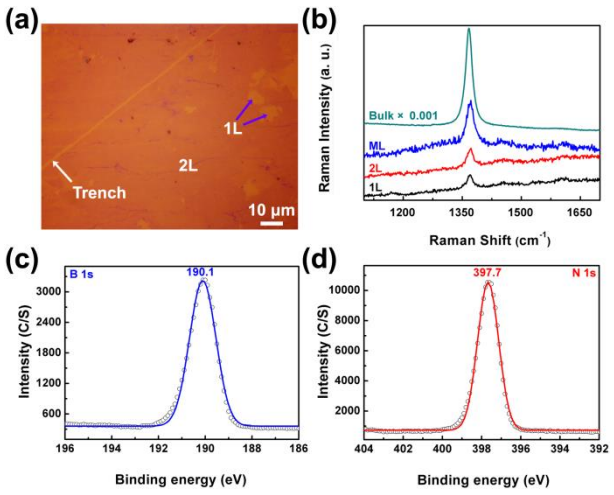

Figure 1. (a) An optical image of 1L and 2L h-BN sheets on a SiO_2/Si substrate containing a trench. (b) Raman spectra of

n-layer h-BN sheets on a SiO_2/Si substrate. XPS spectra of an h-BN film on the silicon substrate: (c) B1s spectrum and (d) N1s spectrum.

XPS characterization was performed to determine the composition and stoichiometric ratio of B:N. The XPS spectra are shown in Figure 1c,d, from which it can be determined that a B1s-core level is present at 190.1 eV (marked in Figure 1c), which is nearly identical to bulk boron nitride with a hexagonal phase that was previously reported[28,29]. The N1s peak is located at 397.7 eV (Figure 1d) very close to the reported position of the N1s spectrum (398.1 eV) of h-BN[28,29]. The stoichiometric ratio of B:N atoms in the h-BN samples was calculated to be ~ 1.10 based on an XPS survey. The slightly higher nitrogen may come from residual nitric acid used for the transfer process.

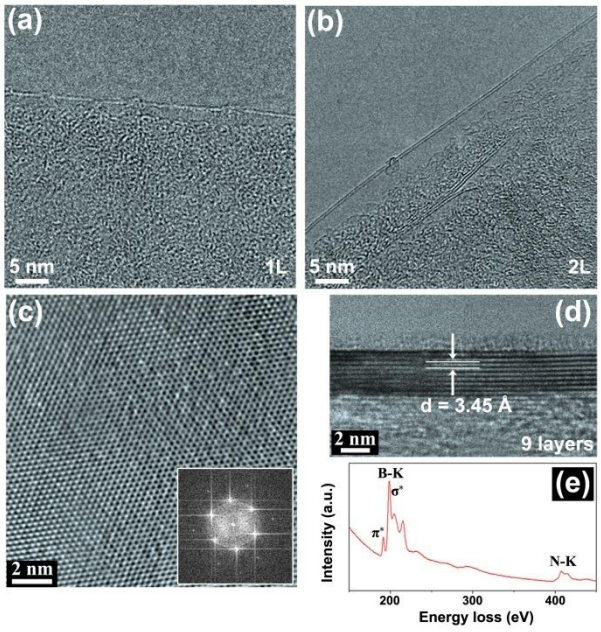

Figure 2. TEM characterization of h-BN films with different thicknesses.(a) High-magnification TEM showing the edge of a 1L h-BN sheet. (b) High- resolution TEM (HRTEM) showing the edge of a 2L h-BN sheet. (c) HRTEM image showing hexagonal atomic arrays as well as its corresponding FFT pattern (shown in the inset) on the h-BN surface, indicating the high crystallinity and quality of the as-grown h-BN samples. (d) HRTEM showing the edge of the investigated h-BN film, which is 9L based on the number of lines at the folding edge. (e) A typical EELS spectra collected on a thin h-BN film.

Transmission electron microscopy (TEM) was performed to characterize the microscopic structures of the h-BN sheets. Figures 2a,b are high-resolution TEM images of 1L and 2L h-BN sheets, respectively. These TEM images further support the suggestion of 1L and 2L h-BN sheets in Figure 1a. Figure 2c shows a high-resolution TEM (HRTEM) image taken from the surface of a few-layer h-BN sheet. The hexagonal lattice can be seen in this image. The corresponding six-fold-symmetry fast Fourier transform (FFT, inset in Figure 2c) pattern confirms the hexagonal structure and multiple layers of h-BN. These results suggest the highly crystalline nature of the h-BN sheet. In its cross-sectional TEM image, shown in Figure 2d, this thin h-BN sheet has ~ 9 atomic layers as determined by the number of lines at the folding edge. The interlayer distance of the h-BN film is ~ 3.45 Å, which is similar to that of bulk h-BN. The electron energy loss spectrum (EELS) is shown in Figure 2e. There are two visible edges starting at ~ 180 and 390 eV, which can be attributed to the characteristic K-shell ionization edges of B and N, respectively[30,31]. In addition, the presence of the characteristic π^* and σ^* energy loss peaks at the boron K edge suggests sp^2-hybridized bonding and a hexagonal structure consisting of B and N in the h-BN samples[30], which is consistent with HRTEM observation of the surface (Figure 2c). The TEM analyses of the h-BN film confirm the single crystal nature of the examined areas and high quality of the as-grown thin h-BN films.

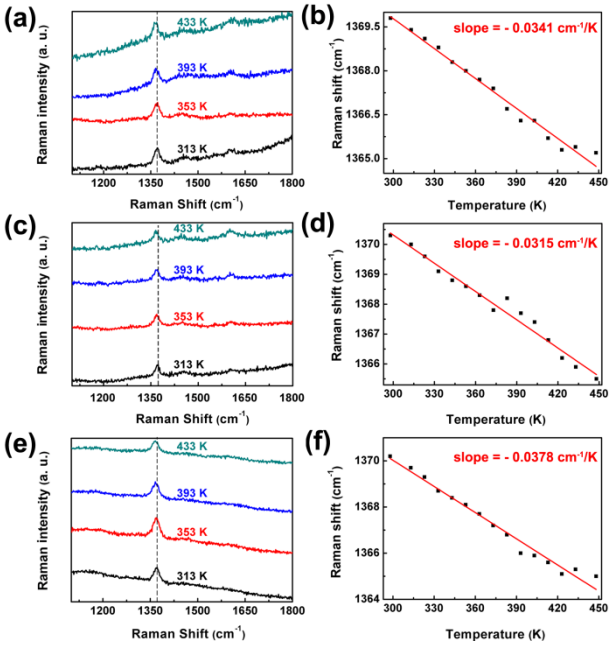

Figure 3. Heating temperature-dependent Raman spectra of 1L, 2L and 9L h-BN sheets. (a,c,e) Raman frequency evolution in the Raman scattering of 1L, 2L and 9L h-BN sheets, respectively, at four temperatures. (b,d,f) The frequencies for the Raman E_{2g} mode in the Raman scattering of 1L, 2L and 9L h-BN sheets, respectively, as a function of temperature, ranging from room temperature to 448 K. The data was fitted using linear functions, as shown by the red lines.

As recently reported, there are two Raman spectroscopic parameters that can be used to evaluate the thermal conductivity of two-dimensional layered materials such as grapheme[32-34] and thin MoS_2 flakes[35]. The first is the first-order temperature coefficient in the Raman scattering of the investigated samples, which can be directly extracted from temperature-dependent Raman spectra and the almost linear relationship between Raman peak frequencies and the surrounding temperature. This coefficient can be obtained by measuring the corresponding Raman spectra of silicon-supported samples with the substrate temperature controlled by an external heating stage (Supporting Information). Figure 3 shows the temperature-dependent Raman spectra of 1L, 2L and 9L h-BN sheets with the substrate temperature ranging from 298 K to 448 K. To ensure the credibility and repeatability of the temperature-dependent Raman data, the relevant Raman spectra were collected as the substrate temperatures were cooled (Figure S3). As shown in Figure 3a, c and e, the Raman E_{2g} modes red-shifts for 1L, 2L and 9L h-BN flakes are detected, which are sensitive to the surrounding temperature due to the B-N bond strength change. As the temperature increased from 313 K to 433 K, red Raman shifts of E_{2g} mode were 4.0 cm^{-1}, 4.1 cm^{-1} and 4.4 cm^{-1} for 1L, 2L and 9L h-BN sheets, respectively. Correspondingly, when the temperature decreased from 433 K to 313 K, blue Raman shifts of E_{2g} modes were observed that were 4.3 cm^{-1}, 3.7 cm^{-1} and 4.1 cm^{-1} for 1L, 2L and 9L h-BN sheets, respectively. These Raman shifts of the E_{2g} mode for different h-BN flake temperature increases and decreases are quite similar. In addition, the peak frequency temperature variation for the E_{2g} modes could be fitted using linear functions, which are shown in Figure 3b, d and f with solid straight lines for 1L, 2L and 9L h-BN sheets, respectively. These results suggest the strong dependence of the E_{2g} mode on the surrounding temperature. In view of similar temperature-dependent Raman behaviors in graphene, the temperature dependence of the E_{2g} mode frequency shift in h-BN sheets can be described by eq 1:

$$\omega(T) = \omega_0 + \chi \times T \quad (1)$$

where ω_0 is the frequency of the E_{2g} mode when the absolute temperature T is extrapolated to 0K and χ is the first-order temperature coefficient. Based on the slopes of the fitted straight lines in Figure 3b, d and f, the relevant first-order temperature coefficients of the E_{2g} modes for 1L, 2L and 9L h-BN sheets could be extrapolated and are $-(3.41 \pm 0.12) \times 10^{-2}$ cm^{-1} K^{-1}, $-(3.15 \pm 0.14) \times 10^{-2}$ cm^{-1} K^{-1} and $-(3.78 \pm 0.16) \times 10^{-2}$ cm^{-1} K^{-1}, respectively.

The other main parameter for the thermal conductivity measurement of h-BN is the dependence of the Raman E_{2g}mode frequency on the excitation laser power.

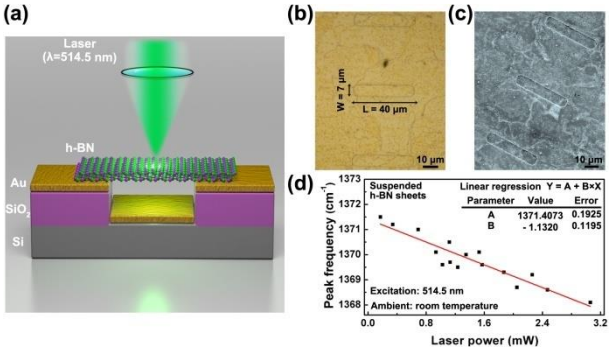

Figure 4. (a) A schematic diagram showing the excitation laser light focused on an h-BN film suspended across a trench. The typical (b) optical and (c) SEM images of a suspended h-BN film(~ 9L). (d) Laser power-dependent peak frequency of Raman E_{2g} mode in a suspended h-BN film.

A schematic diagram of the thermal conductivity measurements by Raman spectroscopy is shown in Figure 4a. To measure the thermal conductivity intrinsic to h-BN flakes by Raman spectroscopy, the samples need to be suspended so as to avoid rapid heat dissipation to the silicon substrate. The silicon substrates were prepared by photolithography and dry etching of Si substrates covered with a 300 nm SiO_2 layer. Prior to the sample transfer, a 150 nm gold film, which served as the heat sink, was thermally

deposited onto the silicon substrate with regular trench arrays. Each trench was a rectangle with a length of 40 μm, a width of 7 μm and a height of nearly 300 nm (Figure S4). Figure 4b and c present the typical optical and SEM images of the h-BN film suspended over the trenches, respectively. From these images, we can find that the h-BN film covers the entire trench area with some production of wrinkles in the film. To ensure that the trench was fully covered by the h-BN film, Raman spectra were collected at different positions across an individual trench. The variation of Raman frequency shifts with the laser power was investigated in detail by tuning the external laser power.

Since the size of the trench is much larger than the spatial resolution of the laser spot (~ 1 μm), the laser can be easily focused in the middle region of the suspended h-BN sheets. Due to the almost negligible thermal conduction of air (~ 0.025 $Wm^{-1}K^{-1}$), the convection losses of laser power to the air for our geometric design is relatively low (~ 0.86 μW). When an external laser is irradiated on the sample surface, the laser energy is partially absorbed (Figure S5), resulting in heat generation in the suspended h-BN that propagates through the extremely thin h-BN film. The laser heating should produce an obvious temperature rise in the central region, which would then be detected on the basis of Raman frequency shifts, as the E_{2g} mode is very sensitive to external heating (Figure 3). The deposited gold film in the trench edge serves as a heat sink such that the temperature is somewhat unchanged when a laser irradiates the sample with low power level. Therefore, the heat generated by the laser irradiation should propagate toward the heat sink.

The heat conduction across any material surface with the areas can be expressed by eq 2:

$$\frac{\partial Q}{\partial t} = -K \oint \nabla T \cdot d\vec{S} \quad (2)$$

where Q is the amount of heat transferred 2-D-dimensional layered materials such as graphene. Given that the radial heat flow propagates from the middle of the suspended flake toward the trench edges, similar to that in few-layer MoS_2[35], the expression for the thermal conductivity of thin h-BN sheets is evaluated in eq 3:

$$K = \chi\left(\frac{1}{2\pi h}\right)\left(\frac{\delta\omega}{\delta P}\right)^{-1}\left(\frac{\delta P_{\mathrm{h-BN}}}{\delta P}\right) \quad (3)$$

where χ is the first-order temperature coefficient extracted in Figure 3, h is the thickness of the h-BN film, ω is the peak frequency shift of Raman E_{2g}mode, $P_{\text{h-BN}}$ is the absorbed laser power by the suspended h-BN film, and P is the external laser power. Using Raman spectroscopy, we have measured the variation of the Raman E_{2g} mode frequency with the external laser power for a number of suspended samples over the trenches. The excitation power over the sample surface was measured with a power meter. Figure 4d presents the frequency shifts of the E_{2g} mode as a function of the incident laser power for a 9L h-BN film, rather than 1L and 2L h-BN sheets. This is because it is still difficult to detect any Raman signals originating from 1L and 2L h-BN sheets when they are suspended over the holes. As shown in Figure 4d, it is evident that, as the laser power increases, theE_{2g} mode frequency shifts toward the lower frequency due to the local laser heating. Considering that the Raman shift is less than 3.4 cm^{-1}, which means a temperature rise of ~90 K in the central region of the sheet, the relationship between Raman frequency shift and external laser power could be described by a linear function, from which we can extract the value of the term from eq 3, namely $\delta\omega/\delta P$ = - 1.13 cm^{-1}/mW. As a result, on the basis of the following parameters: h = 3.0 nm, $\delta P_{\text{h-BN}}/\delta P$ = 10% (Supporting information Part 5, noting that the transmitted light through the h-BN would be mainly reflected from the gold/silicon at the bottom of the trench), the thermal conductivity of 9L h-BN sheets was calculated to be 243 + 37/- 16 $Wm^{-1}K^{-1}$. This value is comparable to that of bulk h-BN, and close to that of 5L h-BN measured by built-in resistance thermometers [23]. This is due to the interlayer coupling in multilayer h-BN, which results in the breaking of the phonon scattering selection rule in 1L h-BN, thus reducing the relevant thermal conductivity values. The values would converge to that of bulk h-BN when the layer thickness is increased to be 5 layers or more [14,36,37]. Also, the obtained thermal conductivity is comparable to that of boron nitride nanotubes reported previously[13]. Even though the thermal conductivity of few-layer h-BN sheets is well-documented by theoretical calculations [14,15],

the experimental confirmation was lacking. Consequently, this finding would be useful in enlarging the applications of h-BN sheets as important components in thermal management.

4. Conclusions

In conclusion, we report the experimental investigation of thermal conduction in suspended few-layer h-BN sheets using a noncontact confocal micro-Raman spectroscopy technique. The room-temperature thermal conductivity of few-layer h-BN sheets was measured to be ~243 $Wm^{-1}K^{-1}$, which suggests that h-BN sheets can outperform silicon oxides as gate dielectric materials with excellent heat conduction. Meanwhile, this study should enlarge the range of h-BN applications as the thermal management material of choice in optoelectronics, photonics, and electronics, and pave the way for efficient thermal management in two-dimensional layered materials.

Acknowledgements

Dr. Haiqing Zhou and Dr. Jixin Zhu contributed equally to this work. This project was supported by the Singapore National Research Foundation under NRF RF Award No. NRF-RF2010-07, the AFOSR MURI (FA9550-12-1-0035), Air Force Office of Scientific Research (FA9550-09-1-0581), U.S. Army Research Office MURI grant W911NF-11-1-0362 and the U.S. Office of Naval Research MURI grant N000014-09-1-1066.

Electronic Supplementary Material: This material is available in the online version of this article at http://dx.doi.org/10.1007/s12274-***-****-*(automatically inserted by the publisher).

References

[1] Kubota, Y.; Watanabe, K.; Tsuda, O.; Taniguchi, T. *Science* **2007**, *317*, 932.

[2] Alem, N.; Erni, R.; Kisielowski, C.; Rossell, M. D.; Gannett, W.; Zettl, A. *Phys. Rev. B* **2009**, *80*, 155425.

[3] Gannett, W.; Regan, W.; Watanabe, K.; Taniguchi, T.; Crommie, M. F.; Zettl, A. *Appl. Phys. Lett.* **2011**, *98*, 242105.

[4] Dean, C. R.; Young, A. F.; Meric, I.; Lee, C.; Wang, L.; Sorgenfrei, S.; Watanabe, K.; Taniguchi, T.; Kim, P.; Shepard, K. L.; Hone, J. *Nat. Nanotechnol.* **2010**, *5*, 722.

[5] Watanabe, K.; Taniguchi, T.; Kanda, H. *Nat. Mater.* **2004**, *3*, 404.

[6] Wang, M.; Jang, S. K.; Jang, W. J.; Kim, M.; Park, S. Y.; Kim, S. W.; Kahng, S. J.; Choi, J. Y.; Ruoff, R. S.; Song, Y. J.; Lee, S. *Adv. Mater.* **2013**, *25*, 2746.

[7] Zhi, C. Y.; Bando, Y.; Tang, C. C.; Kuwahara, H.; Golberg, D. *Adv. Mater.* **2009**, *21*, 2889.

[8] Song, L.; Ci, L. J.; Lu, H.; Sorokin, P. B.; Jin, C. H.; Ni, J.; Kvashnin, A. G.; Kvashnin, D. G.; Lou, J.; Yakobson, B. I.; Ajayan, P. M. *Nano Lett.* **2010**, *10*, 3209.

[9] Lipp, A.; Schwetz, K. A.; Hunold, K. *J. Eur. Ceram. Soc.***1989**, *5*, 3.

[10] Kho, J. G.; Moon, K. T.; Kim, J. H.; Kim, D. P. *J. Am. Ceram. Soc.* **2000**, *83*, 2681.

[11] Chen, Y.; Zou, J.; Campbell, S. J.; Caer, G. *Appl. Phys. Lett.* **2004**, *84*, 2430.

[12] Chang, C. W.; Han, W. Q.; Zettl, A. *Appl. Phys. Lett.* **2005**, *86*, 173102.

[13] Chang, C. W.; Fennimore, A. M.; Afanasiev, A.; Okawa, D.; Ikuno, T.; Garcia, H.; Li, D. Y.; Majumdar, A.; Zettl, A. *Phys. Rev. Lett.***2006**, *97*, 085901.

[14] Lindsay, L.; Broido, D. A. *Phys. Rev. B* **2012**, *85*, 035436.

[15] Ouyang, T.; Chen, Y. P.; Xie, Y.; Yang, K. K.; Bao, Z. G.; Zhong, J. X. *Nanotechnology* **2010**, *21*, 245701.

[16] Shi, Y. M.; Hamsen, C.; Jia, X. T.; Kim, K. K.; Reina, A.; Hofmann, M.; Hsu, A. L.; Zhang, K.; Li, H. N.; Juang, Z. Y.; Dresselhaus, M. S.; Li, L. J.; Kong, J. *Nano Lett.* **2010**, *10*, 4134.

[17] Kim, K. K.; Hsu, A.; Jia, X. T.; Kim, S. M.; Shi, Y. M.; Hofmann, M.; Nezich, D.; Rodriguez-Nieva, J. F.; Dresselhaus, M. S.; Palacios, T.; Kong, J. *Nano Lett.* **2012**, *12*, 161.

[18] Lee, K. H.; Shin, H. J.; Lee, J.; Lee, I.; Kim, G. H.; Choi, J. Y.; Kim, S. W. *Nano Lett.* **2012**, *12*, 714.

[19] Kim, K. K.; Hsu, A.; Jia, X. T.; Kim, S. M.; Shi, Y. M.; Dresselhaus, M. S.; Palacios, T.; Kong, J. *ACS Nano* **2012**, *6*, 8583.

[20] Kim, G.; Jang, A. R.; Jeong, H. Y.; Lee, Z.; Kang, D. J.; Shin, H. S. *Nano Lett.* **2013**, *13*, 1834.

[21] Kubota, Y.; Watanabe, K.; Tsuda, O.; Taniguchi, T. *Science* **2007**, *317*, 932.

[22] Levendorf, M. P.; Kim, C. J.; Brown, L.; Huang, P. Y.; Havener, R. W.; Muller, D. A.; Park, J. *Nature* **2012**, *488*, 627.

[23] Jo, I.; Pettes, M. T.; Kim, J.; Watanabe, K.; Taniguchi, T.; Yao, Z.; Shi, L. *Nano Lett.* **2013**, *13*, 550.

[24] Liu, Z.; Song, L.; Zhao, S. Z.; Huang, J. Q.; Ma, L. L.; Zhang, J. N.; Lou,J.; Ajayan, P. M. *Nano Lett.* **2011**, *11*, 2032.

[25] Ci, L. J.; Song, L.; Jin, C. H.; Jariwala, D.; Wu, D. X.; Li, Y. J.; Srivastava, A.; Wang, Z. F.; Storr, K.; Balicas, L.; Liu, F.; Ajayan, P. M. *Nat. Mater.* **2010**, *9*,430.

[26] Liu, Z.; Ma, L. L.; Shi, G.; Zhou, W.; Gong, Y. J.; Lei, S. D.; Yang, X. B.; Zhang, J. N.; Yu, J. J.; Hackenberg, K. P.; Babakhani, A.; Idrobo, J. C.; Vajtai, R.; Lou, J.; Ajayan, P.

M. *Nat. Nanotechnol.* **2013**, *8*, 119.

[27] Gorbachev, R. V.; Riaz, I.; Nair, R. R.; Jalil, R.; Britnell, L.; Belle, B. D.; Hill, E. W.; Novoselov, K. S.; Watanabe, K.; Taniguchi, T.; Geim, A. K.; Blake, P. *Small* **2011**, *7*, 465.

[28] Park, K. S.; Lee, D. Y.; Kim, K. J.; Moon, D. W. *Appl. Phys. Lett.* **1997**, *70*, 315.

[29] Lee, K. S.; Kim, Y. S.; Tosa, M.; Kasahara, A.; Yosihara,K.; *Appl. Surf. Sci.* **2001**, *169*, 420.

[30] Chopra, N. G.; Luyken, R. J.; Cherrey, K.; Crespi, V. H.; Cohen, M. L.; Louie, S. G.; Zettl, A. *Science* **1995**, *269*, 966.

[31] Mayer, J. C.; Chuvilin, A.; Algara-Siller, G.; Biskupek, J.; Kaiser, U. *Nano Lett.* **2009**, *9*, 2683.

[32] Balandin, A. A.; Ghosh, S.; Bao, W. Z.; Calizo, I.; Teweldebrhan, D.; Miao, F.; Lau, C. N. *Nano Lett.* **2008**, *8*, 902.

[33] Lee, J. U.; Yoon, D.; Kim, H.; Lee, S. W.; Cheong, H. *Phys. Rev. B* **2011**, *83*, 081419.

[34] Cai, W. W.; Moore, A. L.; Zhu, Y. W.; Li, X. S.; Chen, S. S.; Shi, L.; Ruoff, R. S. *Nano Lett.* **2010**, *10*, 1645.

[35] Sahoo, S.; Gaur, A. P. S.; Ahmadi, M.; Guinel, M. J. F.; Katiyar, R. S. *J. Phys. Chem. C* **2013**, *117*, 9042.

[36] Ghosh, S.; Bao, W. Z.; Nika, D. L.; Subrina, S.; Pokatilov, E. P.; Lau, C. N.; Balandin, A. A. *Nat. Mater.* **2010**, *9*, 555.

[37] Lindsay, L.; Broido, D. A.; Mingo, N. *Phys. Rev. B* **2011**, *83*, 235428